ISSN 0915-633X

NATIONAL INSTITUTE FOR FUSION SCIENCE

Impurity Effect in the Quantum Nernst Effect

R. Shirasaki, H. Nakamura, N. Hatano

(Received - Oct. 24, 2005)

NIFS-829 Nov.2005

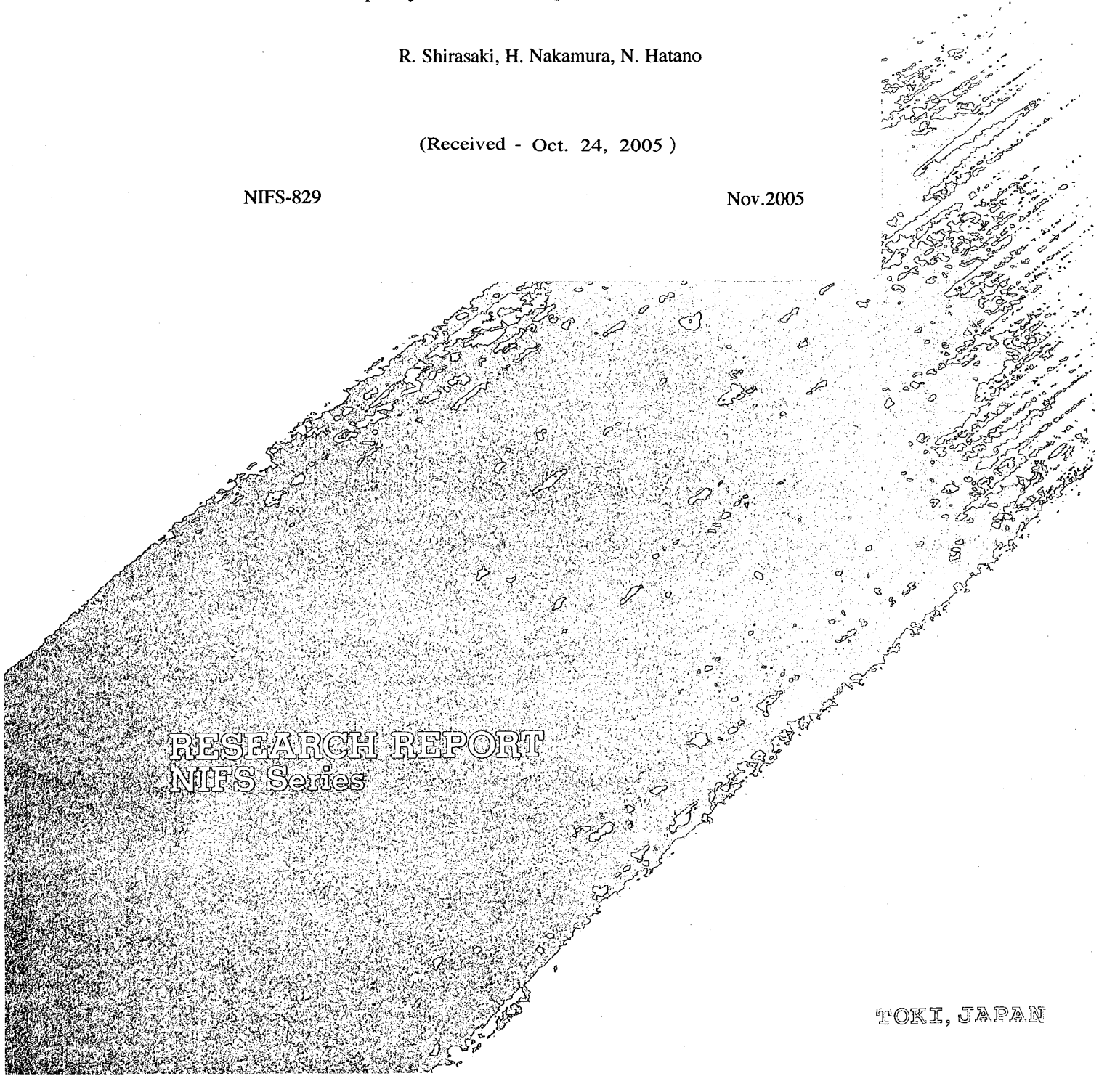

TOKI, JAPAN

Impurity Effect in the Quantum Nernst Effect

Ryōen Shirasaki*
Department of Physics, Faculty of Engineering, Yokohama National University, Tokiwadai 79-5, Hodogaya-ku, Yokohama 240-8501, Japan

Hiroaki Nakamura
Theory and Computer Simulation Center, National Institute for Fusion Science, Oroshi-cho 322-6, Toki, Gifu 509-5292, Japan

Naomichi Hatano
Institute of Industrial Science, University of Tokyo, Komaba 4-6-1, Meguro, Tokyo 153-8505, Japan

We theoretically study the Nernst effect and the Seebeck effect in a two-dimensional electron gas in a strong magnetic field and a temperature gradient under adiabatic condition. We recently predicted for a pure system in the quantum Hall regime that the Nernst coefficient is strongly suppressed and the thermal conductance is quantized due to quantum ballistic transport. Taking account of impurities, we here compute the Nernst coefficient and the Seebeck coefficient when the chemical potential coincides with a Landau level. We adopt the self-consistent Born approximation and consider the linear transport equations of the thermal electric transport induced by the temperature gradient. The thermal conductance and the Nernst coefficient are slightly modified from the pure case and the Seebeck coefficient newly appears because of the impurity scattering of electrons in the bulk states.

Keywords: Models of non-equilibrium phenomena; Green's function methods; Electrical transport (conductivity, resistivity, mobility, etc.); Hall effect; Nano-electronics and related devices

I. INTRODUCTION

The adiabatic Nernst effect in a bar of conductor is the generation of a voltage difference in the y direction under a magnetic field in the z direction and a temperature bias in the x direction (Fig. 1). Each of the left and right ends of the conductor is attached to a heat bath with a different temperature, T_+ on the left and T_- on the right. An electric insulator is inserted in between the conductor and each heat bath, so that only the heat transfer takes place at both ends. A constant magnetic field B is applied in the z direction. Then the Nernst voltage $V_{\rm N}$ is generated in the y direction. In what follows, we always put $\Delta T \equiv T_+ - T_- > 0$ and $B > 0$. The Nernst coefficient is defined by

$$N \equiv -\frac{V_{\rm N}/W}{B\Delta T/L}, \tag{1}$$

where W and L are the width and the length of the conductor bar, respectively.

A classical-mechanical consideration on this Nernst effect yields the following: a heat current flows from the left end to the right end because of the temperature bias; the electrons that carry the heat current receive the Lorentz force from the magnetic field and deviate to the upper edge; then we have $V_{\rm N} < 0$ and $N > 0$. In reality, the Nernst coefficient can be positive or negative, depending on the scattering process of electrons.

We recently studied the Nernst effect in the quantum Hall regime, that is, the Nernst effect of the two-dimensional electron gas at low temperatures, low enough for the mean free path to be greater than the system size

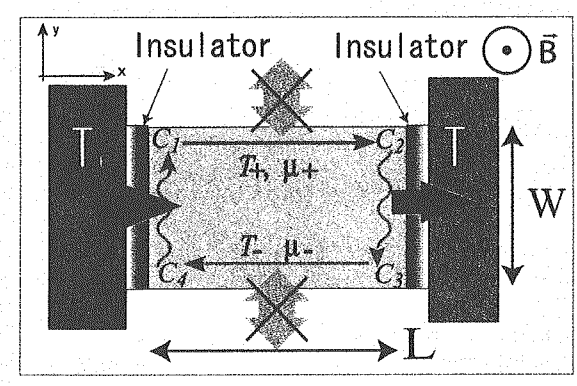

FIG. 1: A setup for observation of the Nernst effect. The Nernst voltage $V_{\rm N}$ is defined as such that it is positive when the voltage of the upper edge is higher than the voltage of the lower edge.

[1]. Using a simple argument on the basis of edge currents [2], we predicted that, when the chemical potential is located between a pair of Landau levels, (i) the Nernst coefficient is strongly suppressed and (ii) the heat current in the x direction is quantized in the unit $\pi k_B^2 T/3h$ when summed over up and down spins. (The quantized unit of the heat current per one spin degree of freedom is $\pi k_B^2 T/6\hbar$.)

However, our previous argument using the edge currents is not applicable when the chemical potential coincides with a Landau level. We must take account of scattering process by impurities and interactions. The bulk states as well as the edge states contribute to the heat conduction and there is influence of impurities on the bulk states. In the present paper, we take account of impurity scattering by adopting the self-consistent Born approximation. We construct the linear transport equa-

*Corresponding author: sirasaki@phys.ynu.ac.jp

tions of the thermomagnetic transport using the current-current correlation functions, which we obtain within the self-consistent Born approximation.

Our conclusions are that (i) the Nernst coefficient and the thermal conductance are slightly modified from the pure case when the chemical potential coincides with a Landau level and (ii) the Seebeck coefficient, which was zero in the pure case, appears due to the impurity scattering. The Seebeck effect is the voltage generation V_S in the direction parallel to the temperature gradient. The Seebeck coefficient is defined by

$$S \equiv -\frac{V_S}{\Delta T}. \tag{2}$$

In the room temperature, the Seebeck coefficient S is positive if the carrier is the hole and is negative if the carrier is the electron [3]. The present calculation shows that the Seebeck coefficient oscillates around zero.

The outline of the paper is as follows: In section II, we briefly explain our convection model, which we introduced [1] to study the Nernst effect in the quantum Hall regime. The construction of the linear transport equation and the self-consistent Born approximation are explained in section III. The numerical result and discussion are given in IV. The final section V is devoted to the summary.

II. CONVECTION OF THE EDGE CURRENT

Let us first briefly explain our model (Fig. 1) that we introduced in our previous study [1]. Since there is no input or output electric current, an edge current circulates around the Hall bar when the chemical potential is in between neighboring Landau levels [2]. The edge current along the left end of the bar is in contact with the heat bath with the temperature T_+ and equilibrated to the Fermi distribution $f(T_+, \mu_+)$ with the temperature T_+ and a chemical potential μ_+ while running from the corner C_4 to the corner C_1. Since the upper edge is not in contact with anything, the edge current there runs ballistically, maintaining the Fermi distribution $f(T_+, \mu_+)$ all the way from the corner C_1 to the corner C_2. It then encounters the other heat bath with the temperature T_- and is equilibrated to the Fermi distribution $f(T_-, \mu_-)$ while running from the corner C_2 to the corner C_3. The edge current along the lower edge runs ballistically likewise, maintaining the Fermi distribution $f(T_-, \mu_-)$ all the way from the corner C_3 to the corner C_4. The Nernst voltage $V_N = \Delta\mu/e \equiv (\mu_+ - \mu_-)/e$ is thus generated, where $e(< 0)$ denotes the charge of the electron.

Our prediction for the pure system was as follows [1]. First, the difference in the chemical potential, $\Delta\mu$, is of a higher order of the temperature bias ΔT, because the number of the conduction electrons is conserved. The Nernst coefficient (1) hence vanishes as a linear response. Second, the heat current in the x direction, $(J_Q)_x$, is carried ballistically by the edge current along the upper and lower edges. The edge current does not change much when we vary the magnetic field B as long as the chemical potential stays between a pair of neighboring Landau levels. The heat current hence has quantized steps as a function of B.

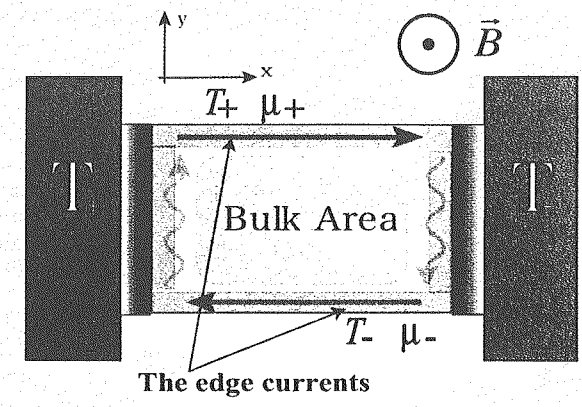

FIG. 2: The geometry of the two-dimensional electron system in a strong magnetic field. We assume that each of the upper and lower edge currents flows maintaining its own temperature all along the edge.

The precise forms of the peaks of the Nernst coefficient and the steps of the thermal conductance in our ballistic model, however, may be different from the reality. This is because our argument using the edge currents is not applicable when the chemical potential coincides with a Landau level. The current is then carried by bulk states as well as the edge states. We thereby need to take account of the effects of the impurity scattering; the impurities strongly affect the bulk state, broadening the Landau levels. We assume that we can separate the contribution of the bulk states from the contribution of the circulating edge currents, which are less affected by the impurity scattering (Fig. 2). In the present paper, we calculate the contribution of the bulk states in the simplest way of considering the impurity scattering.

III. CONTRIBUTION OF THE BULK STATES

In our model shown in Fig. 2, the electrons at each of the upper and the lower edges flow in the x direction maintaining their temperature and chemical potential. Therefore we assume that the temperature gradient *inside the bulk area* is parallel to the y direction:

$$\nabla_x T \simeq 0 \qquad \text{inside the bulk area.} \tag{3}$$

Note that the temperature difference *outside the sample* is normal to the temperature gradient inside the bulk area [1]. In order to obtain the contribution of the bulk states to the Nernst coefficient, we need the ratio between the voltage in the y direction and the temperature gradient in the same direction in the bulk area. The Seebeck coefficient is given by the ratio between the voltage in the x direction and the temperature gradient in the y direction. In the present section, we show the formulation of calculating the voltages from the temperature gradient.

A. FUNDAMENTAL EQUATIONS

We here review some fundamentals. We introduce the particle current density $\vec{J}_n(\vec{r})$ and the heat current density

$\vec{J}_Q(\vec{r})$, given by

$$\vec{J}_n = \left\langle \vec{j}_n \right\rangle, \tag{4}$$

$$\vec{J}_Q = \left\langle (E-\mu)\vec{j}_n \right\rangle, \tag{5}$$

where $\vec{j}_n$ is the particle current operator, μ is the chemical potential and E is the energy of the electrons. Suppose that there are a temperature gradient $\vec{\nabla}T$ and a chemical-potential gradient $\vec{\nabla}\mu$. They work as forces that induce the electric current and the heat current. The linear transport equations are [4]

$$\vec{J}_n(\vec{r}) = -\frac{1}{T}L^{(11)}\vec{\nabla}\mu + L^{(12)}\vec{\nabla}\left(\frac{1}{T}\right), \tag{6}$$

$$\vec{J}_Q(\vec{r}) = -\frac{1}{T}L^{(21)}\vec{\nabla}\mu + L^{(22)}\vec{\nabla}\left(\frac{1}{T}\right), \tag{7}$$

where $L^{(ij)}$ is the transport tensor.

The transport tensor

$$L^{(ij)} = \begin{pmatrix} L_{xx}^{(ij)} & L_{xy}^{(ij)} \\ L_{yx}^{(ij)} & L_{yy}^{(ij)} \end{pmatrix} \tag{8}$$

defined in eqs. (6) and (7) has the following symmetries. Generally, we have the Onsager relation with respect to the reversal of $\vec{B}$: $L_{\alpha\beta}^{(ij)}(-B) = L_{\beta\alpha}^{(ji)}(B)$ [5, 6]. Because of the isotropy of the two-dimensional system, we have $L_{xx}^{(ij)}(B) = L_{yy}^{(ij)}(B)$ and $L_{xy}^{(ij)}(B) = -L_{yx}^{(ij)}(B)$, where the direction of $\vec{B}$ is not changed. From these symmetries, we find the relation $L_{\alpha\beta}^{12}(B) = L_{\alpha\beta}^{21}(B)$.

The tensor element $L^{(11)}$ is given by the current-current correlation function and is a function of the local temperature and the local chemical potential:

$$L_{\alpha\beta}^{(11)} = L_{\alpha\beta}^{(11)}(T,\mu) = \frac{k_{\rm B}T}{\omega_n}\int_0^{1/k_{\rm B}T} d\tau\, e^{i\omega_n\tau}\left\langle T_\tau j_\alpha(\tau) j_\beta(0)\right\rangle. \tag{9}$$

The tensor elements other than $L^{(11)}$ are, within the self-consistent Born approximation, given by integrals of $L^{(11)}$ at zero temperature [6–8]:

$$L_{\alpha\beta}^{(ij)} = L_{\alpha\beta}^{(ij)}(T,\mu) = \int_{-\infty}^{\infty} d\varepsilon\,(\varepsilon-\mu)^{i+j-2}\left(-\frac{\partial f(\varepsilon;T,\mu)}{\partial\varepsilon}\right) L_{\alpha\beta}^{(11)}(0,\varepsilon), \quad \text{for } (i,j)\neq(1,1). \tag{10}$$

B. THE TRANSPORT TENSOR

We now explain the outline of the calculation of the transport coefficients of the two-dimensional electron system including impurities [6–10]. Neutral impurities in the system can be described as a random impurity potential $V_{\rm imp}$. The Hamiltonian in the bulk area is then given by

$$H_0 = \frac{1}{m^*}\left(\vec{p}+e\vec{A}\right)^2 + V_{\rm imp} = \frac{1}{m^*}\left(\vec{p}+e\vec{A}\right)^2 + V_0\sum_i \delta(\vec{r}-\vec{r}_i), \tag{11}$$

where m^* is the effective mass of an electron and $\vec{r}_i$ is the position of an impurity. In the following, we use a measure of the strength of the interaction with impurity, given by

$$\Gamma^2 = \frac{4n_{\rm imp}{V_0}^2}{2\pi l^2}, \tag{12}$$

where $n_{\rm imp}$ is the density of the impurities and l is the cyclotron radius.

We treat the effect of the random potential in (11) by using the self-consistent Born approximation. Although there are various ways of treating the effect of the disorder, we here adopt the simplest approximation. The Green's function of the electron propagation in the Nth Landau level is expressed by

$$G_N(z) = \frac{1}{z - E_N - \Sigma(z)}, \tag{13}$$

where $E_N = \hbar\omega_B\,(N+1/2)$ is the energy of the Nth Landau level and $\Sigma(z)$ is the self-energy with $\omega_B = |e|B/m^*$. The self-energy is given by the diagram in Fig. 3(a). Here the solid line and the dotted line correspond to the electron Green's function and the interaction with an impurity, respectively.

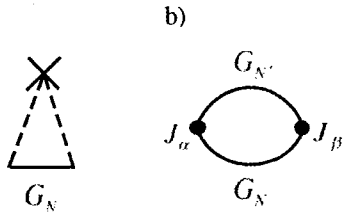

FIG. 3: The diagrams which give the self-energy $\Sigma(z)$ and the current-current correlation function. (a) The self-energy diagram. The solid line and the dotted line correspond to the electron Green's function and the interaction with an impurity, respectively. (b) The diagram for the current-current correlation function. The solid circles correspond to the current J_α, where $\alpha = x$ and y.

The electron Green's function is obtained from the Dyson equation

$$G_N(E) = G_N^0(E) + G_N^0(E)\,\Sigma(E)\,G_N(E), \tag{14}$$

where G_N^0 is the unperturbed electron Green's function $G_N^0(E) = 1/(E-E_N)$. We here make an approximation for a strong magnetic field, or $\Gamma \ll \omega_B$:

$$\Sigma(E) \approx \frac{\Gamma^2}{4}G_{N_0}(E), \tag{15}$$

where N_0 denotes the Landau level closest to the energy E. This is followed by [9]

$$\Sigma(E+i0) \approx \frac{E-E_{N_0}}{2} - i\Gamma\sqrt{1-\left(\frac{E-E_{N_0}}{2\Gamma}\right)^2}, \tag{16}$$

where E_{N_0} is the energy of the Landau level closest to E. In the self-consistent Born approximation, we express Γ

in terms of the relaxation time τ_0, which is obtained in the Born approximation under no magnetic field [10]:

$$\Gamma^2 = \frac{2}{\pi}\frac{\hbar^2\omega_B}{\tau_0}. \tag{17}$$

In the calculation of the transport coefficient (9), we use the diagram for the correlation function, shown in Fig. 3(b). Because we are considering the short-range potential, the vertex corrections are negligible. The transport coefficient is given as follows:

$$\begin{aligned}
&\mathrm{Re}L_{xx}^{(11)}(T,\mu) \\
&= -T\frac{(\hbar\omega_B)^2}{2\pi^2\hbar}\int_{-\infty}^{\infty} d\varepsilon \left(-\frac{\partial f(\varepsilon;T,\mu)}{\partial\varepsilon}\right) \\
&\quad\times\sum_{N=0}^{\infty}(N+1)\mathrm{Im}G_N(\varepsilon+i0)\mathrm{Im}G_{N+1}(\varepsilon+i0),
\end{aligned} \tag{18}$$

and

$$\begin{aligned}
&\mathrm{Re}L_{xy}^{(11)}(T,\mu) \\
&= -T\frac{(\hbar\omega_B)^2}{2\pi^2\hbar}\int_{-\infty}^{\infty} d\varepsilon\, f(\varepsilon;T,\mu)\sum_{N=0}^{\infty}(N+1) \\
&\quad\times\left[\mathrm{Im}G_N(\varepsilon+i0)\frac{\partial\mathrm{Re}G_{N+1}(\varepsilon+i0)}{\partial\varepsilon}\right. \\
&\qquad\left.-\mathrm{Im}G_{N+1}(\varepsilon+i0)\frac{\partial\mathrm{Re}G_N(\varepsilon+i0)}{\partial\varepsilon}\right].
\end{aligned} \tag{19}$$

In the calculation, we should note that the matrix elements of the current operator do not vanish only between the Nth and the $(N\pm1)$th Landau levels and that each Landau level has the $m^*(L\omega_B)^2/(2\pi\hbar)$-fold degeneracy. The transport tensor expressed by eqs. (18) and (19) corresponds to each spin of an electron. The other elements of the transport tensor are given by eq. (10).

C. THERMAL CONDUCTANCE, NERNST COEFFICIENT AND SEEBECK COEFFICIENT

Now that the transport tensor is given, we solve the linear transport equations (6) and (7) under appropriate boundary conditions. In Fig. 2, we have shown our geometry of the two-dimensional electron system in a strong magnetic field. The conductor bar is electrically insulated on all edges and thermally insulated on the upper and lower edges. Hence the boundary conditions of the currents are

$$(J_n)_x = 0 \qquad \text{at the left and right edges,}$$

and

$$(J_n)_y = (J_Q)_y = 0 \qquad \text{at the upper and lower edges.} \tag{20}$$

In order to simplify the equations, we assume that the temperature gradient and the chemical-potential gradient are uniform in the bulk area of the sample. Although the influence of the confining potential appears near the boundaries of the sample, we leave the effect as a future topic.

Solving the equations (6) and (7) with the boundary conditions (3) and (20), we obtain the chemical-potential gradient $\vec{\nabla}\mu$ and the heat current $(J_Q)_x$. The Nernst coefficient is given by

$$\begin{aligned}
N &= -\frac{V_N/W}{B\Delta T/L} = -\frac{L}{W}\frac{\nabla_y\mu}{eB\nabla_y T} \\
&= \frac{L}{W}\frac{1}{eTB}\frac{1}{\left(L_{xx}^{(11)}\right)^2+\left(L_{xy}^{(11)}\right)^2} \\
&\quad\times\left\{-\left(L_{xx}^{(11)}L_{xy}^{(12)}-L_{xy}^{(11)}L_{xx}^{(12)}\right)\frac{K_{xx}}{K_{xy}}\right. \\
&\qquad\left.+\left(L_{xx}^{(11)}L_{xx}^{(12)}+L_{xy}^{(11)}L_{xy}^{(12)}\right)\right\}.
\end{aligned} \tag{21}$$

Note that the temperature gradient *in the bulk area* is given by $\nabla_y T \simeq \Delta T/W$ because of the assumption (3). The Seebeck coefficient is given by

$$\begin{aligned}
S &= -\frac{V_S}{\Delta T} = -\frac{L}{W}\frac{\nabla_x\mu}{e\nabla_y T} \\
&= \frac{L}{W}\frac{1}{eT}\frac{1}{\left(L_{xx}^{(11)}\right)^2+\left(L_{xy}^{(11)}\right)^2} \\
&\quad\times\left\{\left(L_{xx}^{(11)}L_{xx}^{(12)}+L_{xy}^{(11)}L_{xy}^{(12)}\right)\frac{K_{xx}}{K_{xy}}\right. \\
&\qquad\left.+\left(L_{xx}^{(11)}L_{xy}^{(12)}-L_{xy}^{(11)}L_{xx}^{(12)}\right)\right\}.
\end{aligned} \tag{22}$$

The adiabatic thermal conductivity K_Q is given by

$$K_Q \equiv \frac{(J_Q)_x}{\Delta T/L} = \frac{L}{W}\frac{(J_Q)_x}{\nabla_y T} = -\frac{L}{W}\left(K_{xy}+\frac{K_{xx}^2}{K_{xy}}\right), \tag{23}$$

where $K_{\alpha\beta}$ is the thermal conductivity tensor given by

$$\begin{aligned}
K_{xx} &= \frac{1}{T^2}\left\{L_{xx}^{(22)}+\frac{1}{\left(L_{xx}^{(11)}\right)^2+\left(L_{xy}^{(11)}\right)^2}\right. \\
&\quad\times\left(L_{xx}^{(11)}\left(L_{xy}^{(12)}\right)^2-2L_{xy}^{(11)}L_{xx}^{(12)}L_{xy}^{(12)}\right. \\
&\qquad\left.\left.-L_{xx}^{(11)}\left(L_{xx}^{(12)}\right)^2\right)\right\},
\end{aligned} \tag{24}$$

and

$$\begin{aligned}
K_{xy} &= \frac{1}{T^2}\left\{L_{xy}^{(22)}+\frac{1}{\left(L_{xx}^{(11)}\right)^2+\left(L_{xy}^{(11)}\right)^2}\right. \\
&\quad\times\left(L_{xy}^{(11)}\left(L_{xx}^{(12)}\right)^2-2L_{xx}^{(11)}L_{xx}^{(12)}L_{xy}^{(12)}\right. \\
&\qquad\left.\left.-L_{xy}^{(11)}\left(L_{xy}^{(12)}\right)^2\right)\right\}.
\end{aligned} \tag{25}$$

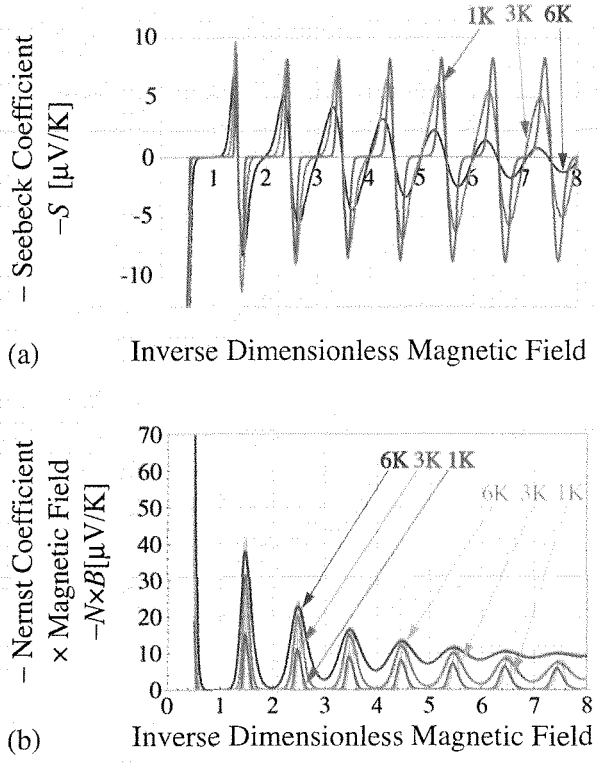

FIG. 4: Scaling plots of (a) the Seebeck coefficient $-S$ and (b) the Nernst coefficient $-N \times B$ both against $m^* \mu/\hbar|e|B$. The red curve, the green curve and the blue curve indicate the results at $T = 1,\ 3,\ 6$ K, respectively. The gray curves in (b) indicate the results of the ballistic transport model [1]. The Seebeck coefficient is always zero in the ballistic transport model.

IV. RESULTS AND DISCUSSIONS

We now present our numerical results. We set the parameters as follows [1]: the effective mass is $m^* = 0.067m_0$ for GaAs, where m_0 is the bare mass of the electron; the relaxation time is set to $\hbar/\tau_0 = 1.0 \times 10^{-4}$eV, which means that the mean free path is 2μm; the sample size is $L = W \simeq 10\mu$m, which is in the same order of the mean free path; the chemical potential is $\mu = 15$meV, which means the carrier density $n_s = 4.24 \times 10^{15}\mathrm{m}^{-2}$.

We calculated the Seebeck coefficient S, the Nernst coefficient N and the thermal conductance $G_Q = K_Q(W/L)$ as shown in Figs. 4 and 5. At low temperatures, the coefficients S and N vanish when the chemical potential is located between the pair of neighboring Landau levels. They appear when the chemical potential is nearly at a Landau level. The Seebeck coefficient S changes its sign rapidly when the chemical potential crosses a Landau level (Fig. 4(a)). In our calculations, the Nernst coefficient N is generally negative and its behavior is similar to the result of the ballistic transport model [1]; the gray curves in Fig. 4(b) are results of the ballistic transport model. The peaks that appear when the chemical potential coincides with a Landau level are broadened by the impurity scattering.

The thermal conductance has quantized steps in the

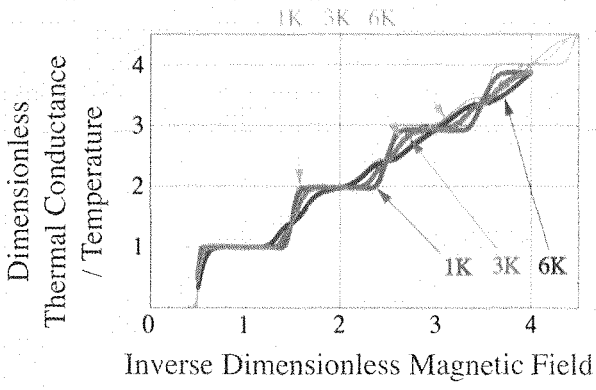

FIG. 5: Scaling plots of $G_Q/T \times 6h/\pi k_B^2$ against $m^* \mu/h|e|B$. The red curve, the green curve and the blue curve indicate the results at $T = 1,\ 3,\ 6$ K, respectively. The gray curves indicate the result at $T = 1.\ 3,\ 6$K in the ballistic transport model.

unit

$$G_{Q0} = \frac{\pi k_B^2 T}{6\hbar} \tag{26}$$

as in the case of the ballistic transport model. (In Fig. 5, the gray curves indicate the results of the ballistic transport model.) It can be interpreted that the heat current is M times a unit current when there are M channels of the edge current.

Incidentally, the ratio between G_{Q0}, the step height of the thermal conductance in our quantum Nernst effect, and the step height of the electric conductance in the quantum Hall effect, $G_0 = e^2/2\pi\hbar$, is

$$\frac{G_{Q0}}{G_0 T} = \frac{\pi^2 k_B^2}{3e^2}. \tag{27}$$

This is consistent with the Wiedemann-Franz law well-known for the Fermi gas.

V. SUMMARY

We discussed a novel quantum effect of the two-dimensional electron gas, in close analogy to the quantum Hall effect. When the chemical potential is between a pair of Landau levels, the edge currents suppress the Nernst coefficient and quantize the thermal conductance. In the present paper, we take account of impurity scattering using the self-consistent Born approximation. The electronic states extend over the system when the chemical potential is close to a Landau level. Then the heat current is carried mainly by the bulk states. As a result, the peaks of the Nernst coefficient and the steps of the thermal conductance are broadened. In addition, the Seebeck coefficient emerges and oscillates rapidly.

Acknowledgments

The authors express sincere gratitude to Dr. Y. Hasegawa and Dr. T. Machida for useful comments

on experiments of the Nernst effect and the quantum Hall effect. This research was partially supported by the Ministry of Education, Culture, Sports, Science and Technology, Grant-in-Aid for Exploratory Research, 2005, No.17654073 as well as by the Murata Science Foundation. N.H. gratefully acknowledges the financial support by the Sumitomo Foundation.

[1] H. Nakamura, N. Hatano and R. Shirasaki: Solid State Comm. **135** (2005) 510.
[2] B. I. Halperin: Phys. Rev. B **25** (1982) 2185.
[3] T. C. Harman and J. M. Honig: *Thermoelectric and Thermomagnetic Effects and Applications* (McGraw-Hill, New York, 1967).
[4] G.D. Mahan: *Many-Particle Physics* 3rd ed. (Kluwer Academic/Plenum Publishers, New York, 2000).
[5] H. B. Callen: Phys. Rev. **73** (1948) 1349.
[6] L. Smrčka and P. Středa: J. Phys. C: Solid State Phys., **10** (1977) 2153.
[7] H. Oji: J. Phys. C: Solid State Phys., **17** (1984) 3059.
[8] H. Akera and H. Suzuura: cond-mat/0409498.
[9] M. Jonson and S. M. Girvin: Phys. Rev. B **29** (1984) 1939.
[10] T. Ando and Y. Uemura: J. Phys. Soc. Jpn. **36** (1974) 959.

Recent Issues of NIFS Series

NIFS-805 P.H. Diamond, S.-I. Itoh, K. Itoh and T.S. Hahm
Review of Zonal Flows
Oct. 2004

NIFS-806 H. Nakamura, N. Hatano and R. Shirasaki
Quantum Nernst Effect
Jan. 2005

NIFS-807 H. Sugama and T.-H. Watanabe
Dynamics of Zonal Flows in Helical Systems
Jan. 2005

NIFS-808 Collection of Contributions from NIFS to 20th IAEA Fusion Energy Conference
(Vilamoura, Portugal, 1-6 Nov. 2004)
Jan. 2005

NIFS-809 K. Itoh, S-I. Itoh, M. Yagi
Self-annihilation of Magnetic Islands in Helical Plasmas
Feb. 2005

NIFS-810 M. Yokoyamna, L. Hedrick, K.Y. Watanabe and N. Nakajima
The Configuration Dependence of Ripple Transport in LHD by the Application of the GIOTA Code
Feb. 2005

NIFS-811 K. Itoh, K. Hallatschek, S.-I Itoh, P.H. Dianmond, S. Toda
Coherent Structure of Zonal Flow and Onset of Turbulent Transport
Feb. 2005

NIFS-812 M.S. Chu, K. Ichiguchi
Effect of the Resisteive Wall on the Growth Rate of Weakly Unstable External Kink Mode in General 3D Configurations
May 2005

NIFS-813 J. García, K. Yamazaki, J. Dies, J. Izquierdo
Internal Transport Barrier Simulation in LHD
June 2005

NIFS-814 T. Watari, Y. Hamada, T. Notake, N. Takeuchi and K. Itoh
Geodesic Acoustic Mode Oscillation in the Low Frequency Range
Sep. 2005

NIFS-815 T. Watari, Y. Hamada, A. Nishizawa, J. Todoroki and K. Itoh
Unified Linear Response Function for the Stationary Zonal Flow and the Geodesic Acoustic Mode
Sep. 2005

NIFS-816 A. Fujisawa, A. Shimizu, S. Ohshima and H. Nakano
A Recipe to Make Zeolite Ion Source for Plasma Diagnostics Beam
Sep. 2005

NIFS-817 A. Fujisawa, K. Itoh, A. Shimizu, H. Nakano, S. Ohsima, H. Iguchi, K. Matsuoka, S. Okamura, S.-I. Itoh and P. H. Diamond
Spectrograph of Electric Field Fluctuation in Toroidal Helical Plasma
Sep. 2005

NIFS-818 H. Wakabayashi, H. Himura, M. Isobe, S. Okamura and K. Matsuoka
Observation of Non-Uniformity of Space Potential on Magnetic Surfaces in Helical Nonneutral Plasmas
Sep. 2005

NIFS-819 H. Sugama and T.-H. Watanabe
Collisionless Damping of Zonal Flows in Helical Systems
Sep. 2005

NIFS-820 T. Tanaka, R. Nagayasu, F. Sato, T. Muroga, T. Ikeda, T. Iida
Comparison of Electrical Properties of Ceramic Insulators under Gamma Ray and Ion Irradiation
Oct. 2005

NIFS-821 S.-I. Itoh, K. Itoh, P.H. Diamond and A. Yoshizawa
Possible Global Magneto-fluid Structure of the Solar Convection Zone
Oct. 2005

NIFS-822 K. Itoh, Y. Nagashima, S.-I. Itoh, P.H. Diamond, A. Fujisawa, M. Yagi and A. Fukuyama
On the Bicoherence Analysis of Plasma Turbulence
Oct. 2005

NIFS-823 T. Nagasaka, T. Muroga, M. Li, D.T. Hoelzer, S. J. Zinkle, M.L. Grossbeck and H. Matsui
Tensile Property of Low Activation Vanadium Alloy after Liquid Lithium Exposure
Oct. 2005

NIFS-824 A. Fujisawa, A. Shimizu, H. Nakano, S. Ohsima, K. Itoh, H. Iguchi, K. Matsuoka, S. Okamura, S.-I. Itoh and P.H. Diamond
Properties of Turbulence and Stationary Zonal Flow on Transport Barrier in CHS
Oct. 2005

NIFS-825 A. Fujisawa, A. Shimizu, H. Nakano, S. Ohsima, K. Itoh, H. Iguchi, Y. Yoshimura, T. Minami, K. Nagaoka, C. Takahashi, M. Kojima, S. Nishimura, M. Isobe, C. Suzuki, T Akiyama, Y. Nagashima, K. Ida, K. Toi, T. Ido, S.-I. Itoh, K. Matsuoka, and S. Okamura
Turbulence and Transport Characteristics of a Barrier in a Toroidal Plasma
Oct. 2005

NIFS-826 S. Ohshima, A. Fujisawa, A. Shimizu and H. Nakano
Development of Zeolite Ion Source for Beam Probe Measurements of High Temperature Plasma
Oct. 2005

NIFS-827 S. Satake, M. Okamoto, N. Nakajima, H. Sugama and M. Yokoyama
Non-local Simulation of the Formation of Neoclassical Ambipolar Electric Field in Non-axisymmetric Configurations
Nov. 2005

NIFS-828 S. Satake, M. Okamoto, N. Nakajima and H. Takamaru
Development of Three-Dimensional Neoclassical Transport Simulation Code with High Performace Fortran on a Vector-Parallel Computer
Nov. 2005

NIFS-829 R. Shirasaki, H. Nakamura, N. Hatano
Impurity Effect in the Quantum Nernst Effect
Nov.2005